Available online at www.sciencedirect.com
SCIENCE DIRECT®
Coordination Chemistry Reviews 249 (2005) 141–160
COORDINATION CHEMISTRY REVIEWS
www.elsevier.com/locate/ccr

Review

Three-dimensional structure determination using multiple-scattering analysis of XAFS: applications to metalloproteins and coordination chemistry

Aviva Levina, Robert S. Armstrong, Peter A. Lay*

Centre for Heavy Metals Research and Centre for Structural Biology and Structural Chemistry, School of Chemistry, University of Sydney, NSW 2006, Australia

Received 3 September 2003; accepted 22 October 2004

Contents

* Corresponding author. Tel.: +61 2 9351 4269; fax: +61 2 9351 3329.
E-mail address: p.lay@chem.usyd.edu.au (P.A. Lay).

0010-8545/$ – see front matter
doi:10.1016/j.ccr.2004.10.008

Abstract

The use of multiple-scattering analysis of X-ray absorption fine structure (XAFS) data for the determination of three-dimensional structures of the active sites of proteins and reactive inorganic species is reviewed, with reference to applications from the authors' research. In particular, the procedures used in the analysis and the advantages and disadvantages of the techniques are described together with a critical evaluation of the information that is obtainable. Particular reference is made to the binding of NO to heme proteins, the structural determination of reactive intermediates in the redox bioinorganic chemistry of Cr, the characterization of anti-inflammatory metal complexes in pharmaceutical preparations, the scattering from hydrogen atoms (first and second coordination shell), and metal dinitrogen complexes.

Keywords: Multiple-scattering; XAFS; Heme proteins; Reactive Cr complexes; Metal anti-inflammatory drugs; Dihydrogen complexes; Dinitrogen complexes

1. Introduction

Extended X-ray absorption fine structure (EXAFS) or X-ray absorption fine structure (XAFS) are somewhat synonymous terms used to describe the oscillations that occur on the X-ray absorption due to the promotion of core electrons into the continuum. The term EXAFS is used specifically to describe the oscillations caused from backscattering of the photoelectron by atoms surrounding the absorbing atom. The term XAFS is gaining more popular usage as it incorporates the oscillations at low energies just beyond the absorption edge rather than just the extended region. This low-energy portion of the XAFS region (XANES [1,2]) is crucial for the multiple-scattering (MS) EXAFS modeling discussed herein, but it also includes atomic XAFS (AXAFS that is not modeled accurately in even the most modern XAFS programs [2]) in addition to EXAFS oscillations. For MS analysis of XAFS data, the AXAFS contributions are usually minimized during the extraction of the EXAFS in order that the fit between EXAFS theory and experiment is optimized. The resulting MS analysis of XAFS data, particularly when used in conjunction with XANES [1,2] and other spectroscopic and structural information, is a very powerful technique for determining the three-dimensional structures of species for which X-ray crystallographic structures are not available. This situation may apply as a result of the instability of the complex/protein and/or the requirement to study the structure in the solution phase. One of the major advantages of MS analysis of XAFS data is the ability to obtain accurate and precise structural information from any medium, so long as only one or two different coordination environments are present in the sample for a given absorbing element. The disadvantage is that XAFS does not provide an absolute determination of a structure. Instead, the structure determination is made on the basis of fitting data to structural models and, therefore, the development of suitable models is crucial. Normally, the number of suitable starting model structures is restricted by consideration of spectroscopic and other information available on the complex or metalloprotein. As such, the analysis can often provide definitive evidence for the presence of one structural type over another, as well as provide accurate and precise bond length and, in many cases, bond angle information. Even if an XRD structure of a metalloprotein is known, MS analysis of XAFS data obtained from frozen solutions is extremely valuable. The relevant merits of protein crystallography and XAFS and combinations of these techniques in studying metalloproteins are given in recent reviews [3–5]. Some examples of why it is important to use XAFS, even if the XRD structure is known, are outlined in the following examples of relevance to the current review [3,6–9].

(i) Usually, metal–ligand bond lengths are an order of magnitude more accurate and precise (0.01–0.02 Å) than those obtained using XRD (typically ∼0.1 Å) [3,6,9], except for the few XRD structures that are determined to a resolution of ∼1 Å.
(ii) Crystallization procedures for XRD structures can sometimes result in active sites that are not biologically relevant due to coordination of ligands from the crystallizing medium, e.g., an ammine ligand [10], or other small molecules/ions used as buffers or to control ionic strength.
(iii) XRD structures performed on crystals where a coordinating molecule is diffused into a preformed crystal are subject to crystal packing forces that can lead to coordination geometries different from those present in the biologically relevant solution structures [7,8,11,12].
(iv) XRD determinations of oxidized (Fe(III), Cu(II), Mo(VI), etc.) metalloproteins are often very susceptible to photoreduction at the metal center during structural determinations, even at liquid nitrogen temperatures, when highly focused synchrotron X-ray beams are used. This often leads to changes in the structural details of the active site, e.g., the NO adduct of ferric nitrophorin 1 (NP1NO) is completely reduced in the X-ray beam [13] although a related complex NP4NO is stable [14].
(v) There is an advantage in having XRD data for calibrating theoretical parameters for XAFS calculations.
(vi) When the XRD structure is unknown but those of related proteins are known (e.g., the native form, if the mutants are being investigated, or a related adduct of a protein) the XRD structure can be used to build a suitable starting model of the active site of the protein with an unknown structure.

With respect to (iv), XAFS has the advantage over XRD since the structures are normally determined at lower temperatures (liquid He for XAS as opposed to liquid N_2 for most XRD experiments) and with a less intense beam. Moreover, photodamage at the metal center is more easily monitored and the affected data rejected in XAFS compared to XRD. Thus the MS analysis of XAFS data should be considered as a complementary technique that, in many cases, can provide additional and more precise and accurate bond length information about the active site of a metalloprotein than does XRD. By contrast, XRD provides detailed structural information on the whole protein that is not obtainable from the analysis of XAFS data [3,4].

In this review, methods are described for performing MS analyses of XAFS data. Applications of such analyses are illustrated with a variety of examples, mainly from our own work, as it is impossible to cover all of the literature in the area within the space constraints of this review. Other reviews of the application of MS techniques can be found elsewhere [3,15–18]. Here specific examples are given for the binding of NO to heme proteins, the structural determination of reactive intermediates in the redox bioinorganic chemistry of Cr, the characterization of anti-inflammatory metal complexes, the scattering from hydrogen atoms (first and second coordination shell), and metal dinitrogen complexes. The limitations, as well as the advantages, of the applications of MS XAFS analyses to these problems are discussed.

2. Three-dimensional structure determination procedures

2.1. Multiple-scattering (MS) processes

As indicated previously, XAFS is the oscillations that occur on the otherwise smooth background of the X-ray absorption spectrum beyond the absorption edge of an element [3,15–22]. The EXAFS component results from destructive and constructive interference between the wavepacket of the photoelectron produced by absorption of an X-ray by the element of interest (Fig. 1), and the backscattered photoelectron waves caused by interactions with atoms that surround the absorbing atom (Fig. 2). Usually, K-edge spectra are recorded, which result from the ejection of a 1s electron, for elements up to the second row of the transition elements. For the lanthanides and beyond, the K edge is too high in energy to be in a convenient energy range for such measurements and it is normal to measure the LIII edge that results from the ejection of a 2p electron. When the photoelectron is backscattered from a single atom back to the absorbing atom, the process is called single scattering (SS). The fitting of calculated XAFS from such processes to the coordination shell of atoms in the observed XAFS can provide information on the number and types of atoms that surround the absorbing atoms, but does not provide any direct determination of the three-dimensional structure. The use of SS analysis of XAFS data has been superseded somewhat by MS analysis. However, SS analysis is still very useful to obtain preliminary information about potential models for subsequent MS analysis, or when the coordination geometry is too complex to obtain three-dimensional information within the determinacy of the data (Section 2.4).

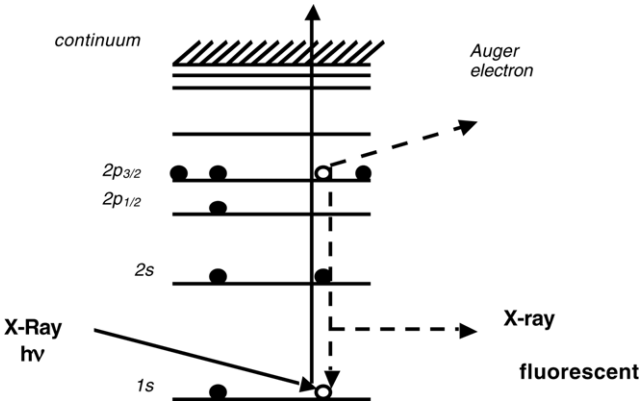

Fig. 1. The X-ray absorption process.

Multiple-scattering analysis of XAFS data includes the calculations of contributions from photoelectrons that are backscattered from two or more atoms (Fig. 2). Generally, the more legs (i.e., numbers of atoms) involved in

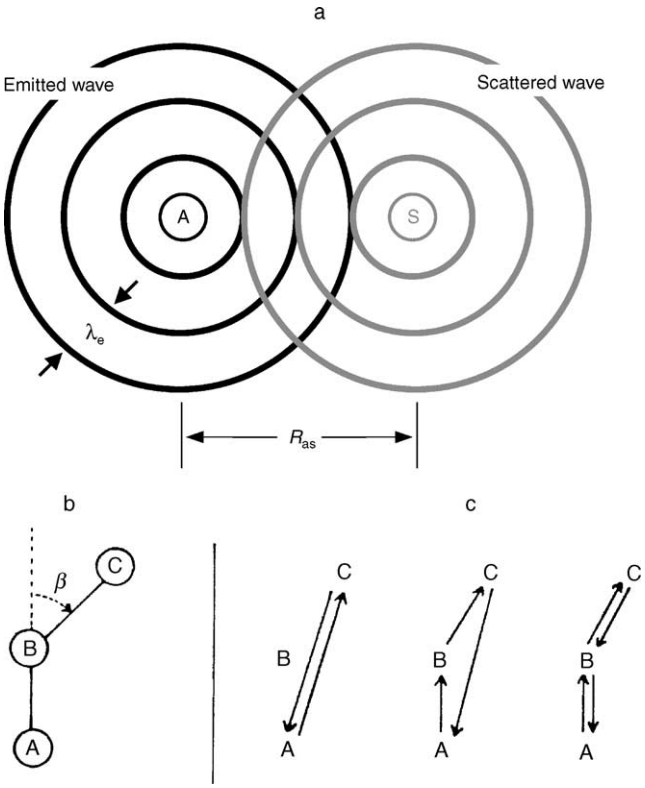

Fig. 2. (a) Interference caused by backscattering of the photoelectron from adjacent atoms that leads to XAFS. Multiple-scattering geometry. (b) Definition of the scattering angle β for a three-atom system (A = absorber; B, C = scatterers). (c) Three possible multiple-scattering pathways.

the backscattering, the weaker is the contribution, as it is dampened by the distance and nuclear motions. However, the most important aspect of MS is that the contribution is strongest when atoms are collinear, and drops off rapidly below 140° [3,15–19,22–27]. This sensitivity enables the determination of angles and, hence, in some complexes, the three-dimensional structure for the first few coordination shells, i.e., to 5–6 Å from the absorbing atom. It is the application of MS analysis that will be the focus of the subsequent sections.

2.2. XAFS data collection and extraction

2.2.1. XAS data collection

Appropriate data collection and treatment are essential in order to maximize the ability to use MS analyses of XAFS data for three-dimensional structure determinations. For this reason, there are a number of things that need to be considered when measuring samples.

For solid samples, the spectrum is measured in absorption mode by ion chambers. Ideally absorption of a sample (A) after the edge is ∼80%. There are programs that allow the absorption of a sample to be calculated, e.g., *Xcom* [28], and these can be used to calculate whether the sample needs to be diluted by a material with a low absorptivity, i.e., BN. The ratio of BN to compound is based on the weighting factor, ρ_t ($g\,cm^{-2}$), which is calculated using Eq. (1).

$$\rho_t = \frac{\ln(1 - A)}{\mu_{pre} - \mu_{post}} \quad (1)$$

Here, μ_{pre} and μ_{post} are the photon attenuation coefficients before and after a certain shell. If the sample is too absorbing, the XAFS will be distorted by higher harmonics (even when the beam is detuned) and other problems will arise due to low photon counts at high k values where the XAFS is weak. These problems will diminish the reliability of the MS fitting procedure. If, on the other hand, there is too little of the absorbing atom in the X-ray beam, then the reliability of the fitting can again be decreased by noise in the data.

As mentioned above, higher-order harmonics contribute to the XAFS for a tuned beam and since these contributions are not calculated in the normal methods of XAFS analysis, it is necessary to remove them (or at least reduce them to insignificant values). Historically, this was achieved by detuning the beam by 50% but, in the most modern beamlines, this is achieved by harmonic rejection using appropriate optics before the beam reaches the sample. The latter is preferable (so long as photoreduction is not a serious problem; see below) since it maximizes the intensity of the beam on the sample and, therefore, provides the best signal-to-noise ratios in the resultant data.

Photoreduction is a serious problem in all synchrotron-based X-ray techniques and arises primarily from secondary effects caused by X-ray-induced ionization of molecules, e.g., water (Eq. (2)). The electron that is released can reduce the absorbing atom and, hence, result in analysis of a coordination environment that differs from that originally present. This reduction process is much more important than photooxidation by, for example, $OH^{\bullet}$, probably due to the ability of the electron to readily diffuse or tunnel through the medium to reach the absorbing atom. This is particularly noticeable for metalloproteins, where most oxidized forms of metalloproteins readily show photoreduction (Cu(II), Fe(III), Mo(VI), etc.). However, most reduced forms, such as Fe(II) and Mo(IV), are extremely stable in the beam and, hence, reliable structures are more easily obtainable.

$$H_2O + h\nu \rightarrow H^+ + OH^{\bullet} + e^- \quad (2)$$

Generally, photoreduction is more serious for species in solutions than in the solid state, and for metalloproteins than for coordination complexes. The problem of photoreduction of samples has increased in importance with the advent of more brilliant sources and focused beams. Indeed, for particularly photosensitive samples, it is often better to gather data over a longer time with a second-generation source or on a bending magnet beamline than one with a more brilliant beam such as that obtained on a wiggler beamline. Because of the adverse effects of photoreduction on the accuracy of structure determinations, the edge position has to be monitored on successive runs and calibrated against the edge energy of a suitable standard during measurements. This allows data that are significantly affected by photodamage to be rejected in the analysis of the XAFS data. Generally, sampling is set up in order that the beam can be moved to a new spot on the sample when photodamage becomes noticeable in order to improve counting statistics in the averaged spectra.

Low temperatures (liquid He temperatures) are desirable for several reasons. The first is that this reduces the extent of photodamage. This improves the quality of the data and, hence, the reliability of the structure determination. The second is that the lower the temperature, the lower the thermal displacements (Debye–Waller factors). Since atomic motion is reduced, the scattering (particularly MS) becomes much stronger and, hence, the determination of the three-dimensional structure becomes more reliable. There is the added advantage that the resolution of shells improves due to the lower Debye–Waller factors. Due care has to be taken, however, when there is the possibility of spin equilibria or other temperature-dependent structural changes. Where there is a spin equilibrium, the lower temperature will favor low-spin complexes, which can result in a changeover to a structure that differs from the predominant high-spin room-temperature structure. This spin-state change is apparent, for instance, when the structure of met-Lb (Lb = leghemoglobin) [29] or met-IDO (IDO = indolamine 2,3-dioxygenase) [30] is determined at liquid He temperature where the low-spin form predominates, as opposed to the high-spin form at room temperature [31,32]. There is one other problem that is in-

herent in using frozen solutions in XAFS analyses, particularly with aqueous solutions, and this is the formation of ice crystals. Such crystals cause two problems; one is that the crystals can result in Bragg reflections that give rise to glitches in the XAS and can make the data unusable. The second is that crystals increase the background scattering of X-rays, which decreases the signal-to-noise ratios. For these reasons, it is often better to use organic solvents that have a tendency to glass or, if aqueous medium is required, a glassing agent such as glycerol is added [6–9]. Care has to be taken, however, that the glassing agent does not coordinate to the element of interest or cause other changes in structure. This should be checked by measuring such properties as the UV–vis absorption spectrum of the metalloprotein or coordination complex in the presence and absence of the glassing agent.

One of the most important requirements for accurate structure determination is to obtain XAFS data over as large a *k* range as possible. This improves the accuracy and precision of the determination of the bond lengths, improves the resolution of shells of atoms that surround the absorbing atom at a similar distance, and improves the determinacy of the analysis of the three-dimensional structure (Sections 2.4–2.6). Important factors that determine the usable *k* range are: the concentration of the absorbing atom; the intensity of the beam; the sensitivity of the detection system (especially for solutions); the degree of photodamage; the number of scans used in the average; and the weighting of the count time for the data points. Generally, the count time per data point is ramped up over the *k* range so that the count time is at least 5–10 times longer at the end of the *k* range compared to the start of the *k* range. This weighting of the count times, reduces the noise at high *k* values and, hence, maximizes the usable *k* range. When LIII edges are measured, there is also the limitation that the values can only be measured up until the LII edge, e.g., to $\leq$18 Å^{-1} for Os (Section 7). While a larger *k* range can be measured for the LI edge that results from the ejection of a 2s electron, the intensity of this edge is much weaker than that of the LIII edge, which decreases the signal-to-noise ratios at high *k* values. Other physical limitations on the useful *k* range are the presence of an adjacent (heavier) element in the periodic table within the sample being measured. For instance, the useful *k* range for the Cu K-edge in many metalloproteins is limited to ~600 eV by Zn contamination.

For solutions and dilute solid samples, the normal method of measurement of the absorption spectrum is to count the fluorescent X-rays. These X-rays are emitted from the absorbing atoms when valence electrons transfer to the core shell vacancies that result from the ejection of the photoelectrons (Fig. 1). Probably the most crucial area for the further development of the application of XAFS to dilute samples is in the detector area. This is far more important than improving X-ray flux, because of the photoreduction problems. With modern beamlines, the signal-to-noise ratio is often limited by the deadtime of Ge detectors (which requires attenuation of the fluorescent photon flux to a maximum value of ~100,000 cps) rather than the intensity of the beam. More recently, software has been developed to correct for deadtime in Ge detectors, which allows the measurement of photon fluxes that are an order of magnitude higher [33]. In summary, for most applications of XAFS for the determination of the structures around the absorbing atoms in metalloproteins and coordination complexes, it has been developments in photon detection that have had the biggest impact and will continue to do so. The photodamage induced by increasing the source flux beyond that available with a second generation source is problematic for standard metalloprotein XAS measurements. It is not simply a matter of obtaining the XAS more quickly; with intense beams, it is often essential that the beam is attenuated during the alignment process used in finding the spots on the sample where the XAFS will be measured. Such attenuation is required to prevent significant photodamage of a precious sample before the XAS is recorded. Alternatively, the samples in these beamlines are aligned by alternative means that do not involve the irradiation of the sample. Where, the third generation sources have the biggest impact is when rapid acquisition of XAFS is required to follow intermediates in reactions, or to study unstable intermediates generated by processes such as photolysis.

It needs to be emphasized that the improvements in fluorescent X-ray detection have been critical to the development of structure determination using MS analyses of XAFS data. The technology has developed from Lyttle detectors, to multi-element Ge detectors (now commonly 30-element Ge detectors). New technology is coming on the scene in order to improve the count rates and hence improve data collection. These developments include Laue-diffraction-based detectors [34] and monolithic Ge pixel detectors, which have been built with up to 100 pixels [35]. The former suffer from the drawback that they are energy (element) specific and, thus, need to be changed when changing elements, but they offer some advantages in being more sensitive than the Ge detectors.

During the measurement of the XAS, the intensity of the beam as a function of energy is measured by an ion chamber before the sample. In both absorption and fluorescence detection modes, the measured intensity of the incident beam is used to normalize the absorption spectrum.

2.2.2. Extraction of XAFS from XAS data

Normally more than one scan is run to obtain the XAS data and these scans are averaged in order to improve the signal-to-noise ratio. This is especially the case for solutions where not only the XAFS scans need to be averaged but also the XAFS data obtained from different channels for a multi-element Ge detector are averaged. The first step in any analysis is to remove data that have been significantly affected by photoreduction, as shown by the XANES. The next step in the analysis of the XAFS data is to average the remaining XAFS data. Normally, the XAFS data that are used in the fitting procedure consist of a weighted average in which

the contribution of each channel or scan is weighted to take into account the absolute intensity of the XAFS and/or the signal-to-noise ratio in the XAFS. Variations in the intensities of the XAS signals emanating from individual channels within a multi-channel fluorescence detector arise from the sensitivity of the individual channel to the X-ray flux, as well as geometric factors. The geometric factors are particularly important when the detector is close to the sample. In this situation, the fluorescent photon flux arriving at the outer elements is much less than those arriving at the inner elements, which is due to the significantly greater distances and less than optimal angle between the detector elements and the sample. During the process of averaging, each channel and each scan is examined to determine whether there are any problems such as low signal intensity or large Bragg reflections that would warrant rejection of data from a given scan/channel. After averaging, a deglitching process is often required due to remove remaining Bragg reflections from the monochromator that arise from incomplete normalization of the XAS data. Such Bragg reflections in the XAFS data are a particular problem with weak signals obtained from dilute solutions. Alternative methods that include deglitching procedures during the splining process are possible [37].

The steps involved in the extraction of the Cr K-edge XAFS data from the measured XAS spectrum are illustrated in Fig. 3 for the Cr(V)–glutathione complex. In this XAS data there is fairly high background absorption because of the high ratio of S atoms compared to the Cr absorber atom [38]. The first step is subtraction of the background absorption in order to reveal the absorption due to the element of interest. The resulting XAS spectrum is normalized to an edge jump of 1.0 (where the edge jump denotes the underlying intensity of the edge after subtracting the XAFS). The next crucial stage is to fit a polynomial spline to the smooth edge absorption. The background absorption is then removed to reveal the XAFS. As can be seen from Fig. 3c, the raw XAFS is rapidly attenuated at high k values and, therefore, the XAFS is multiplied by a power of k (normally k^3) in order to produce XAFS in which the intensity of the oscillations are similar over the entire k range (Fig. 3d). Such k-weighted XAFS are used in the process of fitting the experimental XAFS to the calculated XAFS. The Fourier transform of the XAFS shows the presence of different shells of atoms around the absorbing atom (Fig. 4). The x-axis in the Fourier transform does not correspond to the interatomic distance because there is a phase-shift in the value of r compared to the actual distance. In

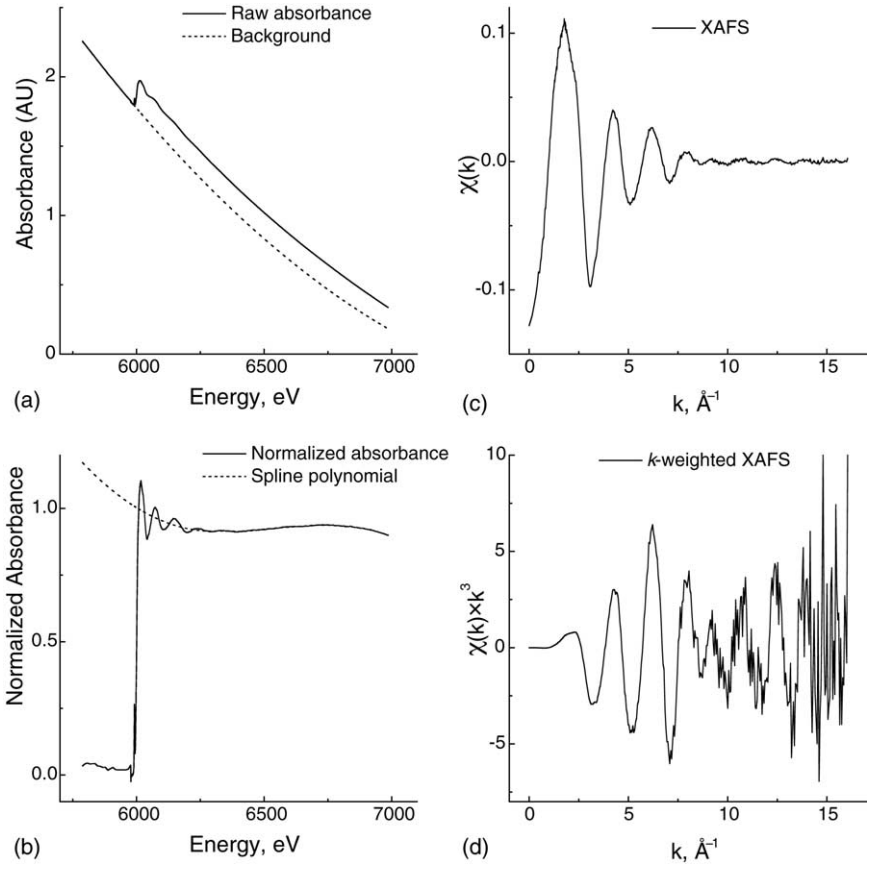

Fig. 3. Data extraction process for analysis of XAFS of solid $Na_3[CrO(LH_2)_2]$ (LH_5 is glutathione) where there is a strong background absorption from the excess S in the isolated complex: [38] (a) subtraction of background absorption; (b) splining to extract XAFS; (c) XAFS; and (d) multiplication of XAFS by a weighting factor (normally k^3) in order to accentuate the oscillations at high k values.

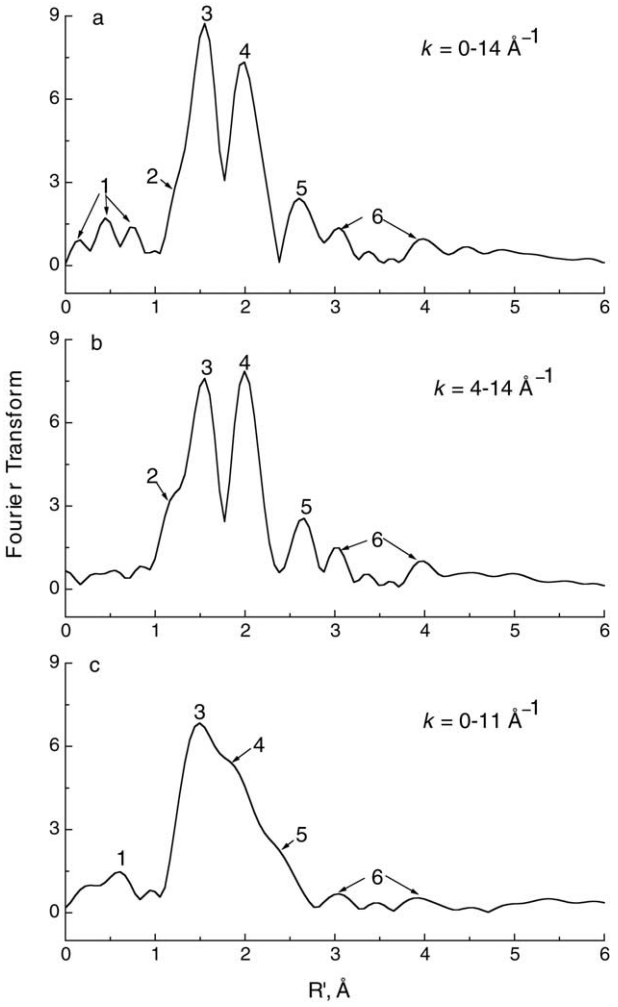

Fig. 4. Influence of limiting the *k* range in XAFS spectrum (Fig. 3d) on the Fourier transform features. An example for the solid $Na_3[Cr^VO(LH_2)_2]$ complex (where LH_5 is glutathione) is used [38]. Designations: 1 is atomic XAFS, 2 is the Cr═O scattering, 3 are the Cr─O/N scatterings, 4 are the Cr─S scatterings, 5 are the Cr···C scatterings (second coordination shell of the *N*,*S*-chelating ligands), and 6 are the MS contributions.

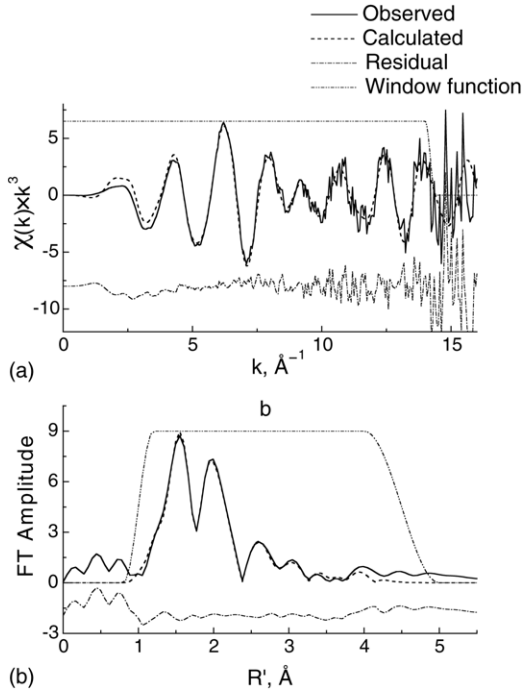

Fig. 5. Typical experimental (unwindowed) and calculated (windowed) XAFS (a) and FT XAFS (b) spectra of the solid $Na_3[Cr^VO(LH_2)]$ complex (where LH_5 is glutathione) at 10 K. Adapted from ref. [38].

some programs, e.g., *XAFSPAK* [39] and *EDA* [40], phase-corrected Fourier transforms can be displayed, which give the actual distances of the atomic shells surrounding the absorbing atoms.

As mentioned previously, it is crucial to have a good spline in order to obtain good calculated fits to the extracted XAFS data. Examination of the Fourier transform is invaluable in determining whether the spline is of sufficient quality to proceed with the analysis of the XAFS. If large peaks are observed at low *r* values before the main peak due to atoms in the first coordination sphere, then the spline procedure has not been optimized in order to remove the atomic XAFS. Where this problem occurs, the spline has to be modified until such contributions are minimized. A poor spline is also evident in some systems by large peaks after the first peak, if there is no reason for such a peak, e.g., a heavy element in close proximity or strong MS contributions. The presence of atomic XAFS and multi-electron transitions at low *k* values [41–43] leads to peaks at low *r* values even when a good spline is used to extract the XAFS data (Fig. 4). More advanced techniques of obtaining the spline and removing both the background and atomic XAFS involve iterative processes in which the smooth background is determined by calculating the atomic XAFS, matching this up with the high frequency oscillations in the Fourier transform and subtracting it from the background [44]. After several such iterations, a reproducible background absorption is obtained and leads to an accurate spline and XAFS that is free of atomic XAFS at low *k* values, i.e., only the EXAFS component is left [44]. While this technique provides excellent EXAFS data at low *k* values, it is a time-consuming process. If atomic XAFS is a serious problem (as evident from the Fourier transform) it is more normally removed by windowing the Fourier transform to remove the low *r* components and back-transforming the data to produce XAFS in which the high-frequency atomic components have been removed (Fig. 5).

2.3. XAFS models and fitting

One of the crucial features in obtaining accurate three-dimensional structures is to minimize the number of variables with respect to the number of independent data points. This is achieved by placing constraints and restraints on pa-

rameters that are fitted in the calculations [24,36]. Invariably the most accurate structures are obtained when the system is highly symmetric and constraints are used to make equivalent or very similar bond lengths and bond angles identical. Constraints are not allowed to vary during the fitting procedures; whereas restraints are placed on parameters such that a bond length or angle is allowed to vary only within a reasonable value that is based on structural information from other sources. Thus bond angles and lengths within a ligand are restrained to within their normal ranges, which prevents the fit from producing unreasonable structures. Similarly, Debye–Waller factors are restrained from going to either unreasonably high or low values, as are the S_0^2 values. The algorithms for such fitting procedures are incorporated into modern versions of FEFF [2,17], EXCURVE [24,45], and GNXAS [46,47], which are used to calculate the XAFS in most software programs. The Debye–Waller factors for the atoms in a given ligand at a given temperature can also be calculated and included in the fitting procedure as constraints in order to reduce the number of variables further. While this may be a valuable method of reducing the number of variables in the fit, care has to be taken in cases where there is static or dynamic disorder, which means that the Debye–Waller factors may not conform to the calculated values. Further improvements in the calculations of appropriate Debye–Waller factors to be incorporated within constrained or more tightly restrained fitting procedures would greatly improve the reliability and speed of convergence of the fitting process. The size of the *k* and *r* ranges are important and they are normally chosen to be as large as the data reasonably allows in order to obtain the most accurate and precise bonding information from the fits to the data. Often the importance of the contributions of the *k* and *r* data to the calculated XAFS is attenuated at the extremes of the ranges. In terms of the upper limits, this attenuation is chosen on the basis of noise in the XAFS, while at lower end of the ranges, it is used to filter out the importance of the contributions of atomic XAFS that are not included in the EXAFS calculations. Care, however, needs to be taken not to strongly truncate or attenuate the data in the low *k* range since this is where the MS contributions to the XAFS are strongest. In fitting procedures, especially for data obtained in the solid state, the *r* range is often truncated at higher values to remove important backscattering contributions from certain counterions (Section 2.7). The upper value of the *r* range is often chosen to be ∼5 Å but in some rigid systems, such as the 1-phenyl C atoms bound in the meso positions of porphyrins, scattering beyond 5 Å can be still quite significant [7]. Another important variable in the fitting process is the weighting [36] that is given to the restraints placed on a model compared to the goodness-of-fit to the XAFS data within the fitting procedure. For related complexes, the appropriate weighting to be used is determined by running trial MS fits to the XAFS data for a compound with an accurately known structure. Weightings that reproduce the crystal structure are those that are appropriate for the particular structural class. The appropriate weighting varies with the type of ligand system that is being studied, i.e., the more rigid the ligand system, the more appropriate it is to have the restraints weighted more heavily than the goodness-of-fit to the experimental data. The final parameters that are chosen are the number of legs that are included into the fit to the data. For most systems some pathways involving up to five legs make significant contributions (≥10% of the importance of the most important scattering pathway) and, therefore, are included in the calculations. In a significant number of cases, the inclusion of MS pathways often does not affect the accuracy of the determination of the bond lengths (involving the coordinating atoms to the absorbing atom) compared to SS analysis when the coordination shells are well separated, i.e., greater than the SS resolution (Section 2.6). However, MS analysis of XAFS data is essential to make the determination of the nature, distance and angles involving the outer shells reliable and, hence, provide meaningful information on the nature of the donor groups. MS calculations are also essential in the determination of M–L bond distances of shells that cannot be resolved by SS analysis (Section 2.6). In some systems, pathways involving six legs also make significant contributions to the XAFS, but the cut-off of five-leg pathways is normally the compromise made in order to minimize the calculation time while still having a very good fit to the experimental data. Many programs allow users to choose only a few major paths for the MS calculations. While this can reduce calculation times, it is more likely to lead to errors in bond lengths and angles that are determined from MS analyses. This problem arises because there are a large number of SS and MS paths that contribute to the overall XAFS beyond the first peak (coordination shell) in FT of the XAFS. While the absolute magnitude of the sum of all of the scattering from these paths is often much greater than that due to the first coordination shell, most of these paths cancel due to their different phases. Therefore, just choosing only a few MS paths in the EXAFS calculations can lead to less reliable MS analysis of the XAFS data. As such, calculations that include all MS paths within the *r* range window produce more reliable structures and provide greater confidence in the accurate differentiation of M–L bond lengths that differ by less than the SS resolution.

2.4. Determinacy, statistical significance and errors

A crucial factor in the fitting procedure is to ensure that there are more independent data points than there are variables. The determinacy of the system (N_i/p) is calculated from the estimated number of independent data points collected in the XAFS data set (N_i), and fitted parameters included in the model (p), where N_i is given by Eq. (3) [24].

$$N_i = \left[\frac{2(r_{max} - r_{min})(k_{max} - k_{min})}{\pi}\right] + \sum D(N-2) + 1 \quad (3)$$

Here, r_{max}, r_{min} and k_{max}, k_{min} are the maximum and minimum values used in the FT and XAFS filtered data, respectively; D is the number of dimensions within a restrained part of the model (i.e., three for a three-dimensional model); and N is the number of independent atoms within the restrained group of the model.

The N_i/p ratios in MS analysis of XAFS data cannot be compared with the ratio of observations versus variables in X-ray crystallographic refinements. The XRD refinement procedures fit the positions and thermal factors of all non-hydrogen atoms to the observables, without relying on robust starting models, as is the case for MS analysis of XAFS data. Thus XRD requires a ratio of observations over variables that is at least greater than four for a reasonable analysis and a unique fit. On the other hand, a high ratio of observables/variables for a MS analysis of XAFS would be two (and typically much lower). The reason why such analyses work is that highly restrained models are used in MS analyses that incorporate information from a variety of sources, including bond lengths and angle information on chelates that has been obtained from XRD structures of related complexes or proteins. Thus the atoms are not free to move independently from one another and many of the variables are restrained to within physically meaningful values, such that only the metal–ligand bond lengths have complete freedom to move (and often metal–ligand bond angles). Such constraints and restraints not only prevent the XAFS fit from converging to chemically unreasonable structures, it also results in efficient calculation times. The initial stages of the fitting procedure hence involve a considerably overdetermined problem in which only a few bond lengths (normally the movement of a relatively rigid ligand group of atoms) and Debye–Waller factors have freedom to move independently in order to fit the most significant part of the XAFS oscillations (corresponding to the main peak in the Fourier transform). In the final stages of the fitting procedure, all bond lengths, angles and Debye–Waller factors, within their restraints where appropriate, are optimized until the fits reach convergence. Because the fit is optimized to a pre-determined model that is consistent with all of the chemical information known about the species of interest, it is necessary to build a series of all such appropriate models, then optimize the fits to each model. The goodness-of-fit and other parameters that come out of the best fits to a series of structures normally provide a unique solution to the problem, or at least one structure that is much more likely than the rest. The strategy of MS fitting of XAFS data with restrained models can allow meaningful fits to be made even when the N_i/p value is just over one, if the types of ligands in the coordination environment are known precisely by other means.

Methods for error analysis and fitting procedures have been surveyed and evaluated by the International XAFS Society on web publications [48,49], but a few pertinent comments are given below. *XFIT* [36], which was used in the analyses reported herein, monitors the progress of the fitting procedure by means of the residual, R, in the same way as used in XRD refinements. The value of R is calculated from Eq. (4).

$$R = \left(\frac{X^2}{X^2_{\text{calculated}\equiv 0}} \right)^{1/2} \tag{4}$$

In this equation, X^2 is the function minimized in the MS XAFS fit and is defined by Eq. (5) for restrained models, and $X^2_{\text{calculated}\equiv 0}$ is the value of X^2 when the calculated XAFS is uniformly 0.

$$X^2 = X^2_{\text{xafs}} + \sum_{\text{restraint}} X^2_{\text{restraint}} \tag{5}$$

X^2_{xafs} and $X^2_{\text{restraint}}$ are defined by Eqs. (6) and (7).

$$X^2_{\text{xafs}} = \int_{k=0}^{\infty} \{w[\chi_{\text{obs}}(k) - \chi_{\text{calc}}(k)]\}^2 \, \mathrm{d}k \tag{6}$$

$$X^2_{\text{restraint}} = \left(\frac{\Delta_{\text{restraint}}}{\sigma_{\text{restraint}}} \right)^2 \tag{7}$$

In these equations, w is the weighting factor; $\chi_{\text{obs}}(k)$ and $\chi_{\text{calc}}(k)$ are observed and calculated filtered XAFS curves; $\Delta_{\text{restraint}} = 0$ if the restraint expression is satisfied or is the difference between the two sides of the restraint expression otherwise; and $\sigma_{\text{restraint}}$ is the σ value given for the restraint (default value = 1).

Other workers [24] define R by Eq. (8).

$$R = \sum_{i}^{N} \left(\frac{1}{\sigma_i} \right) [|\chi_{\text{obs}}(k_i) - \chi_{\text{calc}}(k_i)|] \times 100\% \tag{8}$$

where

$$\frac{1}{\sigma_i} = \frac{k_i^n}{\sum_i^N k_j^n \{[|\chi_j^{obs}(k_j)|]\}^2} \times 100\% \tag{9}$$

The absolute index of the goodness-of-fit, ε_ν, which takes into account the degree of overdeterminacy in the system is given by Eq. (10).

$$\varepsilon_\nu^2 = \left[\frac{1}{N_i - p} \right] \left(\frac{N_i}{N} \right) \sum_{i}^{N} \left(\frac{1}{\sigma_i^2} \right) [\chi_{\text{obs}}(k_i) - \chi_{\text{calc}}(k_i)]^2 \tag{10}$$

In this equation, N is the number of points in k space. Taking the approach from *XFIT* to calculate R (defined by Eq. (4) above), the value of ε_ν^2 is calculated from Eq. (11).

$$\varepsilon_\nu^2 = \left[\frac{1}{N_i - p} \right] \left(\frac{N_i}{N} \right) R^2 \tag{11}$$

Using this absolute goodness-of-fit, the Fisher's $F_{0.95\%}$ test can be used to determine which of two fits with different numbers of variables, or different k and/or r ranges, are superior. The criterion to be used is that a second fit defined by $(\varepsilon_\nu^2)_{\text{fit2}}$

is better than the first fit defined by $(\varepsilon_\nu^2)_{\text{fit1}}$ if the following condition applies (Eq. (12)).

$$\frac{(\varepsilon_\nu^2)_{\text{fit1}}}{(\varepsilon_\nu^2)_{\text{fit2}}} > F_{0.95\%} \tag{12}$$

In determining whether this condition applies, tabulated values of $F_{0.95\%}$ [40] are used. The application of this methodology for differentiating between four- and five-coordinate models for Cr(VI) thiolato complexes has been described recently [50]. Care has to be taken in its application, however, because a chemically meaningful better fit may be obtained that does not meet the above criteria of statistical significance. This is because significant changes in the fits to second and third shells in the Fourier transform between two models, may not be statistically significant according the Eq. (12) because of the dominance of the first shell to the XAFS. Such situations can arise when comparing the fits to optimized models in which one position in the coordination sphere has two different possible ligands (e.g., when a sixth ligand in a metalloprotein is uncertain) or that have more than one conformation or isomer. A more rigorous approach to statistical analysis is to use a model in which the bond lengths and Debye–Waller factors of the first coordination sphere of the well-defined ligands (such as a heme group) are constrained. The *R* values are then compared between optimized fits to models that incorporate alternative sixth ligands. The new *R* values that are obtained with these constrained fits lead to smaller *p* values and hence ε_ν^2 values and a better discrimination of whether one model is an improvement over another. Nonetheless, criteria other than statistical significance need to be taken into account in deciding whether one fit is better than another, as outlined in Section 2.5.

Errors are also treated in different ways by different researchers. There are three basic sources of errors in the final parameters obtained from fitting procedures. These are systematic errors, errors due to the noise in the data, and the degree of precision to which the bond lengths and angles are reliably determined, which is dependent on the quality of the starting models, and the size of the usable *k* and *r* ranges. Conservative estimates of systematic errors are 0.02 Å in bond lengths [19], but our experience is that when XAFS-derived bond lengths are compared with accurate and precise XRD structures that differences are often 0.01 Å or better for good XAFS data. Errors introduced by noise in the data can be determined by Monte-Carlo analyses [36]. Finally, the reliability of the determined bond lengths and bond angles can be estimated by observing changes in the fit with systematic changes in the parameter of interest. Consideration of all three sources of error has been described elsewhere [6–8,24], but these are only estimates. The degree to which a MS XAFS analysis can reproduce bond angles and lengths in model complexes, where accurate and precise XRD structures are known, is probably the best indication of inherent errors in the determination of related structures.

2.5. What is a good fit?

There are various methods for the determination of the goodness-of-fit, but generally a fit is considered good if the *R* value is less than 20% [24]. Caution has to be taken with such an approach as an absolute measure of the quality of the fit, however, because the value of *R* will decrease if the *k* range is truncated at low values or high values. There are many reports in the literature where the *k* range is truncated at low values in order to improve the MS fit to the XAFS data, because this eliminates AXAFS that are not fitted within the EXAFS theory. While this may be appropriate for SS analysis, it is inappropriate for MS analysis, as the MS contributions to the XAFS are most important at low *k* values. Similarly, while truncation of XAFS data at high *k* values will improve the goodness-of-fit due to removal of noisier data at high *k* values, it also decreases the resolution of shells of backscattering atoms and, hence, the precision and accuracy of the bond length and angle information that is obtained from the fit to the data. In summary, truncation of the *k* range may lead to a better fit, as measured by the *R* value, but results in a less certain and accurate determination of the three-dimensional structure about the absorbing atom. Thus XAFS data should not be truncated at low *k* values in MS fitting procedures.

Apart from the goodness-of-fit parameter, the values of S_0^2 should be 0.9 ± 0.1 [36] for a good fit. Values of S_0^2 that are too high or too low indicate that the actual coordination number is lower or higher than that in the model. Similarly, it is often possible to distinguish between models where the best fits have similar *R* values by examination of the Debye–Waller factors of all of the atoms in the model. If the Debye–Waller factors are unreasonably low ($\leq 0.0005\,\text{Å}^2$) then the model is not a good one and conversely, high values of the Debye–Waller factors ($\geq 0.02\,\text{Å}^2$) are indicative of either a poor fit due to an incorrect model, or disorder within the structure.

2.6. How well can MS analysis of XAFS distinguish between similar M–L bond lengths?

The resolution of absorber–scatterer distances (shells) in SS scattering analysis is given by Eq. (13) [18].

$$\Delta R \geq \frac{\pi}{2\,\Delta k} \tag{13}$$

This limit on the resolution of distances arises because the larger the *k* range, the greater the separation of the individual oscillations at the end of the *k* range. While this equation is often quoted, the resolution of the peaks in the FT corresponding to different shells improves as the temperature is lowered due to reduction in the Debye–Waller factors, so it should only be taken as a reasonable guide. Thus the use of as large a *k* range as possible not only improves the determinacy of the problem, but it also improves the precision and accuracy to which individual metal–ligand bond lengths are determined, and whether individual bond lengths

can be resolved. With the typical *k* ranges used in SS XAFS analysis, M–L bond differences have to differ by 0.1–0.2 Å for the oscillations in the XAFS to be sufficiently resolved to distinguish between these two bond lengths. By contrast, MS analysis of XAFS data has the ability to distinguish between metal–ligand bond distances that differ by a factor that is less than the ∼0.1 Å limit imposed by the SS resolution, provided that the groups to which the ligand donor atoms are attached have quite different MS contributions, which is often the case. The differentiation of M–L bond distances that are less than the resolution obtainable with SS analysis relies on the MS contributions of other atoms within the ligands, since these normally have sufficiently different frequencies of oscillations in the XAFS so that they can be resolved.

The MS contributions are most important in the low *k* range [18] and hence, the most accurate and precise bond length determinations in terms of resolution of different shells (and three-dimensional structural determination) will be obtained when both a large *k* range and all of the low *k* range data are used in the fitting procedure.

2.7. Scattering from counterions in the solid state

One of the features of solid-state XAFS is that counterions are often within 5 Å of the scattering atom and can make very significant contributions to the XAFS. For this reason, the fits to structures in the solid state often have higher *R* values than for the same complexes in solution, even though the XAFS for the latter often have higher noise. Where the position of the counterions are known, these outer-sphere effects can be modeled [51], however, the usefulness of XAFS is that it can be used to determine the three-dimensional structures of unknowns, even when the positions and details of the counterions are uncertain. For these reasons, the following factors should be considered when determining the XAFS structures for unknown solid samples. If the complex with an unknown structure is charged, then for optimal fits, the counterions should consist of light cations, such as Li^+, $NR_4{}^+$, Na^+, Mg^{2+}, or light anions, oxoanions, F^-, etc. Otherwise, the XAFS should be taken in both the solid-state and solution. Similarly, ordered solvent molecules of crystallization can make significant contributions to the XAFS in the solid state. In solutions, both outer-sphere solvent molecules and counterions are less ordered, even in frozen solutions and, hence, their contributions to the XAFS are less important as their Debye–Waller factors are much larger. Nonetheless, there are significant SS and MS contributions from the second solvation sphere in some circumstances, e.g., the second solvation sphere in aqua complexes [52,53].

For metalloproteins, the protein generally protects the metal environment from significant outer sphere effects, although caution needs to be taken with buffers and ions used in the crystallization process so that they do not enter the active pocket in a way that results in derivatives that differ from the active site. Normally, this is checked by determining appropriate spectroscopic signatures of the metal ion of interest in the medium in which the XAS is recorded. This is an advantage of the analysis of XAFS data over XRD structure determinations, since it is often not possible to compare accurately the spectroscopic signatures of solutions with those of crystals.

3. Heme proteins

3.1. MS contributions to the XAFS of heme proteins

Heme proteins are particularly attractive to study by XAFS because symmetry constraints can be applied to the porphyrin to reduce the number of variables. In addition, the relatively rigid nature of the heme group results in strong MS contributions and, together with the importance of this class of proteins in biochemistry, this had led to many studies of heme proteins. The strong SS and MS contributions of the porphyrin, together with the high symmetry results in considerable accuracy and precision in the determination of the average $Fe–N_p$ bond lengths. The contributions due to the strong MS pathways of the heme group create their own problems, however, because they tend to be much more important than the contributions due to the axial ligands. Hence, considerable care needs to be taken in the MS analysis of the XAFS data in order to obtain reliable structure determinations. It is not possible to review the extensive studies in this area within the space limitations of this article, so we will concentrate on a few examples from our own work.

3.2. Met and deoxy heme proteins

Our initial studies concentrated on determining accurate and precise bond lengths in deoxy- and met-Mb (Mb = myoglobin), which included a detailed analysis of the errors inherent in the XRD-determined bond lengths (typically ≥0.1 Å) [6]. At the time the XAFS were reported, very-high-resolution XRD structures (∼1-Å resolution) were not available in the literature. The bond lengths determined by our XAFS studies were subsequently confirmed by XRD studies (at ∼1-Å resolution) that were performed with comparable accuracy and precision [54,55], which established that the MS models used to analyze the XAFS of heme proteins were robust. Importantly, the XRD results confirmed the XAFS results that accurate Fe-His bond lengths could be obtained even when the difference in the $Fe–N_p$ and $Fe–N_\varepsilon$ bond lengths were less than the resolution of bonds obtainable by SS analyses.

XAFS studies have also been performed on Lb [29,56], with similar results for the structures of the deoxy forms of Mb and Lb. By contrast, there were distinct differences in the $Fe–N_p$ bond lengths in the structures of the met- forms of Mb and Lb at 10 K. These differences arise because met-Lb

is predominantly in a bis(His) form at 10 K [31], whereas met-Mb exists as a high-spin heme with an aqua ligand in the proximal site at both room temperature and at 10 K. Thus, the Fe–N_p bond lengths for met-Lb at 10 K (2.00 Å) are typical of low-spin Fe(III) (**I**), compared to the longer bond lengths observed in met-Mb (2.05 Å) (**II**) [6] and the AcO^- adduct of Lb (2.04 Å) (**III**) [29,56] that remain in the high-spin forms at 10 K.

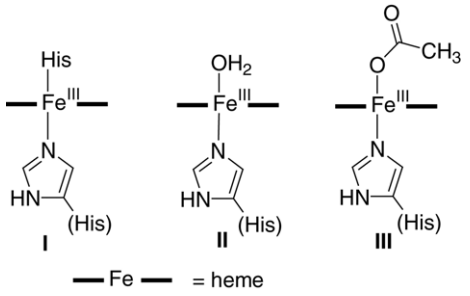

3.3. Cytochrome c

In order to understand the reasons for the fast electron-transfer reactions of cytochrome *c* in terms of inner-sphere reorganizational energy, it was important to obtain accurate and precise bond lengths in both the Fe(III) and Fe(II) oxidation states. The MS analyses of XAFS data from the two oxidation states enabled the Fe-ligand bond lengths to be determined more precisely than those reported in the literature for the XRD structures [9]. Such MS analyses of XAFS data showed that the changes in the bond lengths and bond angles about the Fe center were smaller than those estimated from the less precise and less accurate Fe–L bond lengths obtained from the XRD structures [9]. In the XAFS-derived structures (**IV**), neither the Fe–N_p and Fe–N_ε bond lengths changed (i.e., differences were 0.01 Å) on changing the Fe oxidation state, while the Fe–S bond only decreased by 0.04 Å in going from Fe(III) to Fe(II).

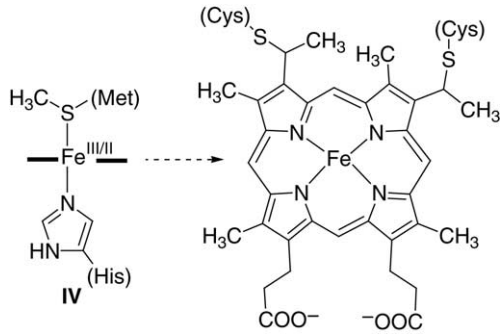

3.4. NO adducts

The binding of NO to heme proteins has been an area of intense recent interest because of the diverse roles of NO in biology and medicine, many of which involve the formation of NO bonds to heme proteins [57–60]. The first applications of MS analysis of XAFS data to determine the Fe–NO bond lengths and Fe–N–O bond angles in non-heme systems appeared in 1995 [26,27]. This prompted our studies on NO adducts of heme proteins, which was directed to the investigation of whether bonding information could be obtained from NO adducts of Fe(II) and Fe(III) hemes [7,8]. In all of the systems studied to date, the adducts of Fe(II) proteins have Fe–NO bond lengths (1.72–1.77 Å) and bond angles (145–155°) that are typical of Fe(II) model complexes. For the Fe(III) protein adducts, all of the Fe–NO moieties are nearly linear with a Fe≡NO triple bond (1.66–1.68 Å, best described as Fe(II)–NO^+, Fig. 6). Similar Fe–NO geometries were obtained from MS analysis of XAFS data obtained from the NO adduct of ferri-cyt *c* [61] and the Fe(II) and Fe(III) adducts of IDO, except the IDO adducts are five-coordinate [30,62]. The small range in Fe–NO bond distances and Fe–N–O bond angles for adducts of a given Fe

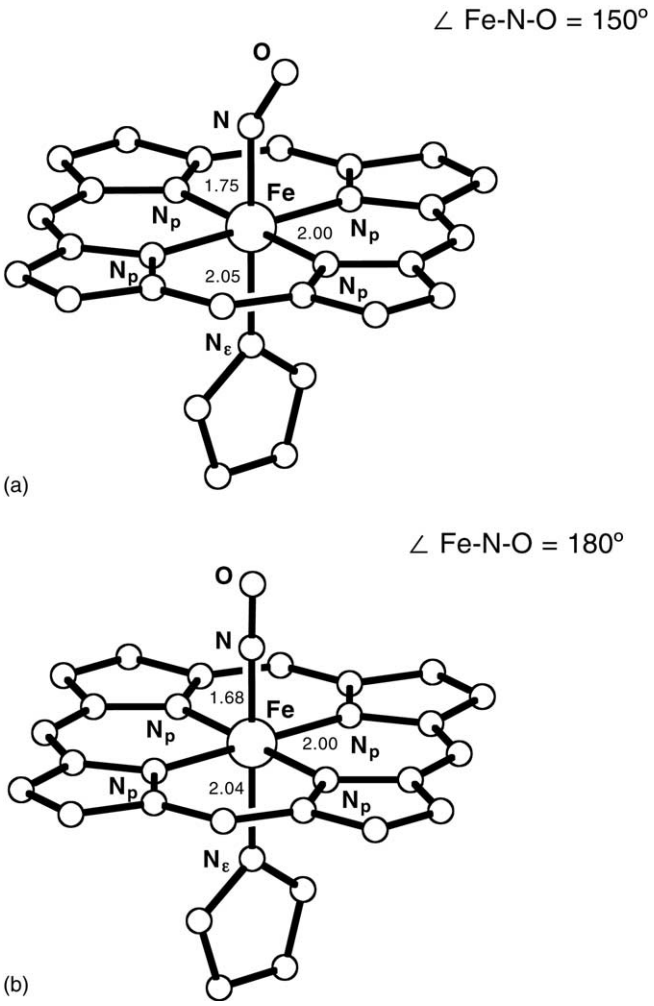

Fig. 6. Molecular structures of the active sites of horse heart (a) Mb^{II}–NO and (b) Mb^{III}–NO at 10 K.

oxidation state in heme proteins is consistent with XAFS-[7,63,64] and XRD-derived [65,66] data from many heme model complexes. By contrast, we and others have argued that the large variations in such bonding parameters that have been obtained in protein crystallography are due to a combination of: (i) NO diffusion into preformed crystals, which can give non-equilibrium bonding geometries due to crystal packing forces; and (ii) the larger errors that are inherent in bond distances in most XRD structures compared to XAFS-derived structures of the heme. Further support for our assertion that the binding geometry in Mb^{II}–NO and Hb^{II}–NO (Hb = hemoglobin) is virtually the same (as is Lb–NO), can be found in the solution Raman spectra, which are virtually the same with respect to the energy of the bands due to the Fe–NO modes. This can only be explained by similar bond angles in the Fe–NO moiety [67].

4. Reactive chromium species

4.1. Chromium XAS: biochemical applications

One of the major developments in Cr biochemistry has been the application of MS analysis of XAFS data in order to determine the three-dimensional structures of reactive species of relevance to Cr-induced cancers [68,69]. While many of these reactive species are short-lived, they can be produced in a pure form in solutions and then rapidly frozen or rapidly precipitated from solution. This methodology has provided an enormous amount of information on the structures of such species in the complex redox chemistry of Cr.

Since the structures of Cr complexes obtained from MS analysis of XAFS data can be correlated with different XANES spectra, they can also be used to study the structures of Cr complexes within cells. The high spatial resolution of modern X-ray microprobe beamlines [70] will enable mapping by XANES of Cr complexes within cells, and micro-XANES has already been used to study the reduction of Cr(VI) in whole cells [71]. The combination of intracellular mapping by XANES with three-dimensional structures determined by MS analysis of XAFS data is likely to provide unprecedented information on biologically relevant biotransformation processes.

4.2. Chromium(VI)

Apart from simple Cr(VI) species such as chromate and dichromate, most Cr(VI) species are reactive intermediates in Cr redox reactions with organic substrates and are too unstable to be crystallized for analysis by single-crystal diffraction. However, some Cr(VI) thioesters with biomolecules, such as glutathione, can be generated in solution in a pure form and their structures have been determined by MS analysis of the XAFS data obtained from frozen solutions [50]. In the case of Cr(VI) thioesters, the XAFS and XANES differ in aprotic, non-aqueous solvents compared to those in water. Together with electronic absorption spectroscopy data, the XAS results showed that the complexes exist as an equilibrium between a four-coordinate (**V**) and five-coordinate (**VI**) species as shown below. Species **VI** is likely to be an important intermediate in Cr-induced cancers [50].

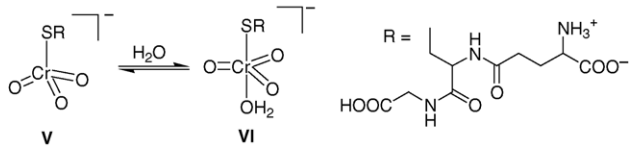

V VI

4.3. Chromium(V)

While there is an increasing number of Cr(V) complexes that have been characterized by X-ray crystallography [68,69], most of the complexes are too unstable to be crystallized. Their structures have been determined, however, by analysis of XAFS data from solid-state samples (rapidly precipitated powders) or from frozen solutions. The most studied Cr(V) systems are those prepared from 2-hydroxycarboxylates (**VII**). The structures of the hmba (**VIIa**) and ehba (**VIIb**) complexes have been determined by X-ray crystallography [72,73]. The bond lengths determined from MS analysis of XAFS data in the solid state and solution [74,75] are the same as those in the crystal structures of **VIIb**. The work has been extended to characterize the Cr(V) complex with quinic acid (**VIIc**) [76] and the complexes where R = Me and R′ = *t*-Bu or *i*-Pr [77]. MS analysis of XAFS data can also be applied to mixtures of two different Cr species, which has been very useful in the characterization of the Cr(V) citrate complex (**VIId**). This unstable complex co-precipitates with the Cr(III) citrate complex, but MS analysis of XAFS data was used to determine simultaneously the structures of the Cr(V) and Cr(III) complexes in the mixture [78]. All of the Cr(V) 2-hydroxycarboxylate complexes were also characterized by EPR spectroscopy and XANES and the similarity of their spectral properties was consistent with the XAFS determinations of similar structures for all of these complexes. While the Cr–O(oxo) bond is easily distinguished with certainty from the other four Cr–O bonds by SS analysis, it is only by application of MS analysis of XAFS data that the Cr–O(carboxylato) and Cr–O(alcoholato) bond lengths can be distinguished, since the difference in bond lengths is less than the resolution of the SS analysis [75]. This analysis is complicated somewhat by the presence of geometric isomers in solution, but since the angles involving the 2-hydroxycarboxylate chelates and the Cr absorber remain essentially constant in the different geometric isomers, this does not compromise the differentiation of the Cr–O(carboxylato) and Cr–O(alcoholato) bonds [75].

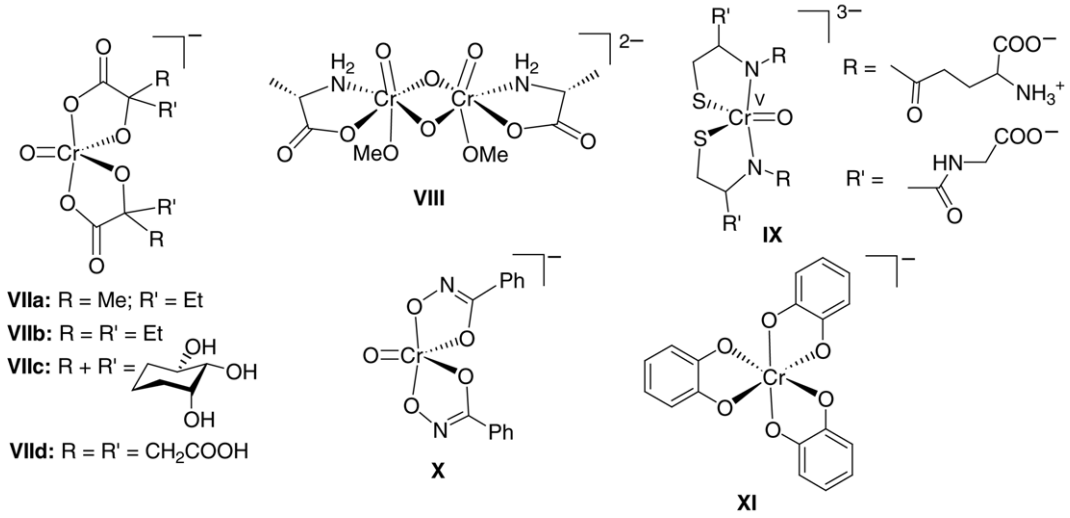

The first structural characterization of a Cr(V) amino acid complex (**VIII)** has also been obtained by MS analysis of XAFS data [79]. In addition, a number of Cr(V) peptide complexes have been characterized, including the Cr(V) glutathione complex (**IX**, Figs 3–5) [38], as well as a range of non-sulfur-containing peptide complexes [77,80,81]. Hydroxamic acid complexes (such as **X**) have also recently been characterized by MS analysis of XAFS data and they also exhibit a typical five-coordinate oxochromate(V) structure with two of the chelating ligands [82]. The XAFS-derived structure of *cis*-$[Cr^{V}(phen)_2(O)_2]^{+}$ (phen = 1,10-phenanthroline) [51] has short Cr–O bonds (1.63 Å) and much longer Cr–N(phen) single bonds (2.04 and 2.16 Å). The Cr(V) catecholato (cat) complexes (**XI**) are rare examples of Cr(V) complexes that do not contain either an oxo or nitrido ligand. Structures of such complexes have been assigned as $[Cr^{V}(cat)_3]^{-}$ (with a significant π-electron delocalization between the metal ion and the ligand), rather than $[Cr^{III}(cat)(sq)_2]^{-}$ (where sq = 1,2-semiquinonato(1−)) [83], based on XAFS, XANES, and spectroelectrochemical data (Section 4.7).

4.4. Chromium(IV)

Chromium(IV) species are very reactive, with only a very few species being stable enough to crystallize for XRD analysis, but they are also of importance as reactive intermediates in Cr redox chemistry of relevance to Cr-induced cancers and oxidation reactions of organic substrates [68,69]. A range of Cr(IV) complexes with 2-hydroxycarboxylic acids (such as **XIIa–c**) can be prepared in essentially 100% yield by the As(III) reduction of Cr(VI) in the presence of the ligand [84,85]. Moreover, these Cr(IV) complexes are stable enough in solution to undergo ligand-exchange reactions with other ligands such as picolinate and oxalate [85]. Since pure solutions of these complexes can be prepared, they can be rapidly frozen and their structures determined by MS analysis of XAFS data. The ehbaH complex, R = R′ = Et, has similar Cr=O(oxo) and Cr=O(carboxylato) bond lengths as the Cr(V) analogue, but the alcohol donor is no longer deprotonated and the Cr–O(alcohol) bond is now ∼0.2 Å longer than the corresponding bond in the Cr(V) complex [74,75]. Structures of the oxalato and picolinato complexes, $[CrO(ox)_2]^{2-}$ and $[CrO(pic)_2]$, have also been determined by MS analysis of the XAFS data [86]. The generation of Cr(IV) peptide and catecholato complexes is described in Section 4.7.

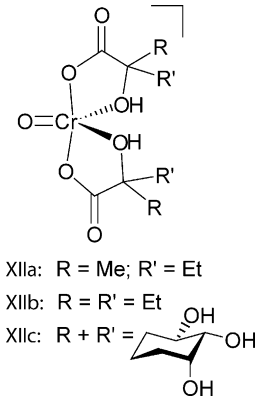

4.5. Chromium(III)

Generally, the structures of Cr(III) complexes are determined by XRD [87], but some complexes, particularly those with peptides, are difficult to crystallize and XAFS is also useful for determining the structures of Cr(III) species in solution. For instance, the $[Cr^{III}(ehbaH)_2(OH_2)_2]^{+}$ product from the reduction of the Cr(V) and Cr(IV) analogs was also analyzed by MS analysis of XAFS data, which showed that the Cr–O(carboxylato) and Cr–O(alcohol) bond lengths differ little from the Cr(IV) complex, with the main structural changes being the replacement of one short Cr=O bond with two much longer Cr–OH_2 bonds [74,75].

Attempts have been made to determine the structure of chromodulin [88], which is purported to be the biologically

active form of Cr in insulin activation, although this is still under dispute [69]. The presence of more than one Cr sites, together with a range of poorly defined potential donor ligands, does not allow meaningful MS analysis of the XAFS data to be performed at present; hence, only SS analysis has been performed [88]. The analysis of the Cr(III) catecholato species in the redox series is reported in Section 4.7.

4.6. Chromium-nitrosyl complexes

There has been considerable controversy with regard to the oxidation states of Cr nitrosyl complexes, which have been recently studied by XAS [89]. The XAFS indicate the complexes are best described as Cr(I)–NO^+ complexes with considerable π backbonding. The effective charge at the Cr center, as judged by XANES, is between those typically observed for Cr(II) and Cr(III) complexes. The power of MS analysis of XAFS data for discriminating between geometric isomers was demonstrated for *trans*-[Cr(NO)(acac)$_2$(OH$_2$)], where it was established that the fit to the XAFS data was much better for a *trans* isomer model (**XIII**) than for a *cis* isomer model. The *trans* structure determined from the analysis of the XAFS data is also consistent with other spectroscopic evidence [89].

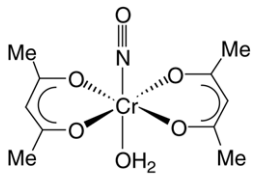

XIII

4.7. Electrochemical XAFS

Electrochemical XAFS cells have been designed by different research groups and have allowed electrochemical studies to be performed simultaneously with XAS experiments [63,64,90–95]. Such techniques are useful for the determination of the structures of unstable and/or air-sensitive oxidation states of the metal in complexes and proteins. The electrochemical cells are also useful for the maintenance of the redox state of complexes that are susceptible to photoreduction or photooxidation in solution, since a potential can be chosen to keep the compound of interest in the appropriate redox state.

Chromium catechol complexes are of interest because the reactions of Cr(VI) with catechols produce Cr(V) species that cause DNA damage. These processes may model some reactions that occur in vivo [96–98]. Catechol complexes are also of interest because of their unusual magnetic properties [99–103] and their rich redox chemistry makes them ideal for study by XAS spectroelectrochemistry. Both the XANES and the XAFS of $[Cr(cat)_3]^{n-}$ (n = 1–3) complexes indicate that the redox chemistry for the first two oxidations to produce $[Cr(cat)_3]^{2-}$, and $[Cr(cat)_3]^{-}$, respectively, is metal-centered rather than ligand-centered, which contradicts what was generally believed to be the case [99–103] before these XAS studies. The first two oxidations (Cr(III) → Cr(IV) and Cr(IV) → Cr(V)) result in a significant shift in the Cr K edge position to higher energies. In addition, the Cr–O bond lengths decrease by a similar amount in the successive oxidations as those observed for the V–O bond lengths in the crystallographically characterized V(III/IV/V) catecholato series [83,104]. In systems where the redox chemistry is definitely ligand-centered, e.g., $[Cr(tren)(3,6\text{-dtbcat})]^{2+/+}$ (tren = tris(2-aminoethylamine), 3,6-dtbcat = 3,6-di-*tert*-butylcatecholato(2−)), the Cr–O bond lengths increase on oxidation of the complex [105], which further supports our contention that the redox chemistry is metal centered for the oxidation reactions of the $[Cr(cat)_3]^{n-}$ series (n = 1–3). On further oxidation of $[Cr^{V}(cat)_3]^{-}$ to the "$[Cr(cat)_3]^{0}$" complex, the edge energy and shape revert back to being similar to those of $[Cr^{III}(cat)_3]^{3-}$ and the Cr–O bond length increases, which is consistent with a Cr(III) complex with three oxidized (semiquinone) ligands [104].

The Cr(V/IV) redox chemistry of certain Cr(V) complexes of non-sulfur-containing peptides is reversible, which has enabled XAFS studies of Cr(V) and Cr(IV) peptide complexes with the same ligands [80]. Complex **XIV** maintains a very similar five-coordinate structure in both oxidation states, with the main difference being a slight increase in the average Cr–L bond length on reduction from Cr(V) to Cr(IV) [80].

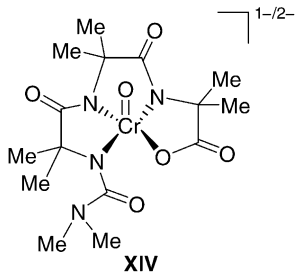

XIV

5. Metal complexes as anti-inflammatory drugs

Copper(II) and Zn(II) complexes of indomethacin are potent anti-inflammatory drugs with reduced side-effects compared with the parent organic drug. They are already in use as veterinary anti-inflammatory drugs and are potential new human drugs [106,107]. These complexes exist as a dinuclear paddlewheel Cu(II)-acetate type structure with four bridging carboxylato ligands (**XV**), or as monodentate complexes with unsymmetric chelating carboxylates [106–110]. The distinctive scattering contributions of the second metal, in the case of the dimers, and of the fairly rigid carboxylate MS contributions for both classes of complexes, makes MS analysis of XAFS data a reliable technique for determining their structures. Indeed MS analyses of XAFS data [111–114] repro-

duce accurately the structures of crystallographically characterized [108–110] Cu(II) and Zn(II) complexes, and have been used to determine the structures of new indomethacin complexes of Cu(II) [111,112], Ni(II) [114] and Co(II) [114] that have yet to be crystallized. The Ni(II) complexes can be dimers or monomers depending on the nature of the solvent from which they are precipitated, whereas the Co(II) complexes are always monomers [114]. In addition, it has been shown by XRD powder diffraction that the Zn(II) monomer complexes precipitate as a mixture of the crystallographically characterized octahedral *cis*-$[Zn(Indo)_2(ROH)_2]$ (R = Me or Et) complexes and another species with the same formula. Both powder XRD and XAFS show that this second phase is not a dimer and mixed-models have shown that the mixture consists of the octahedral *cis*-$[Zn(\eta^2\text{-}O,O'\text{-}Indo)_2(ROH)_2]$ and the tetrahedral $[Zn(\eta^1\text{-}Indo)_2(ROH)_2]$ complex [113]. This again shows the power of XAFS in determining the structures of unknowns in mixtures of complexes.

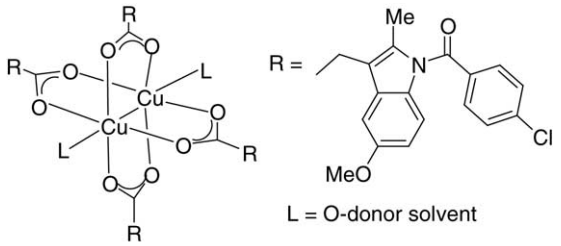

XV

The work on these anti-inflammatory drugs also highlights another advantage of MS analysis of XAFS data over other structural methods in that studies can be performed directly on the complexes in pharmaceutical preparations and biological fluids [112].

6. Is hydrogen important in XAFS analysis?

6.1. Scattering from second coordination sphere O–H or N–H protons

Hydrogen atoms are normally not included in analyses of XAFS data because their contributions are expected to be very small compared to heavier elements such as C, N or O around the absorbing atoms. While this approximation is normally reasonable, there are a number of situations where H atoms can make significant contributions. Consider for instance, hexaaqua complexes, where the short O–H bonds place the H atoms reasonably close to the absorbing atom (<3 Å). With 12 H atoms at approximately the same distance in such complexes, the H atoms have a similar scattering power as two equivalent C atoms at that distance. Of course, the scattering will be somewhat smaller due to the fact that all of the atoms are not at identical positions, especially in the solid state, but this will be offset somewhat by the much greater number of MS paths involving 12 H atoms in the second coordination sphere as compared to 2 C atoms at an equivalent position. The contribution of aqua ligands to the XAFS has been evaluated in detailed studies of hexaaqua complexes, which has shown that such contributions cannot be ignored completely [53]. The effect is even greater for ammine complexes, e.g., hexaammine complexes where there are 18 equivalent H atoms equal in scattering to 3 C atoms at the same distance, and pentaammine complexes where there is a set of 12 equivalent H atoms in the *cis* coordination sites and another 3 H atoms at a similar distance arising from the *trans* ammine ligand [115]. While MS contributions have yet to be assessed, addition of SS contributions of these H atoms greatly improves the fits of XAFS data of ammine complexes [115] and MS effects are expected to be significant.

6.2. Scattering from first coordination shell hydrido and dihydrogen ligands

One of the challenges in structural inorganic chemistry is to determine the structures of dihydrogen and hydride complexes, particularly the position of the hydrogen atoms, because of the small contributions of hydrogen atoms to the diffraction of such species. The need for developing new structural methods lies in the importance of these species in industrial catalysis [116,117]. Koningsberger et al. have performed extensive experimental and theoretical studies on the contributions of Pt–H bonds in Pt particles of relevance to catalysis [116,117]. Such bonds make considerable contributions to both the AXAFS and the EXAFS in the low *k* range of the XAFS and enable both the position of the H atoms on the clusters and the Pt–H bond distances to be determined. However, the Pt–H EXAFS is rapidly attenuated with an increase in the *k* value and is insignificant beyond values of $\sim 2\ Å^{-1}$, which again highlights the importance of using the whole XAFS *k* range for meaningful analysis of data. Given the significant contributions of H atoms in the second shell mentioned above, and to Pt–H bonds in Pt particles, it was also expected that significant XAFS contributions would be observed from coordinated dihydrogen ligands in metal complexes. The question remained, however, as to whether H–H bond distances could be determined given the acute M–H–H bond angles in dihydrogen complexes, since such a geometry would be expected to result in weak M–H–H MS contributions (Section 2.1).

In order to test this possibility in a series of complexes with a range of H–H bond lengths, we conducted a study of the Os–H_2 amine/ammine complexes that have been well characterized by Taube and coworkers [118]. Indeed, both the Os–H and H–H bond distances could be reproduced in MS analysis of XAFS data from a complex for which the neutron structure was known. In addition, there was a good correlation of the H–H bond distances determined by XAFS in a series of complexes with the distance deduced from proton NMR experiments, which gave further confi-

dence in the analysis [115]. For example, the Os–H and H–H bond lengths (1.60 Å and 1.30 Å, respectively) determined from the MS analysis of the XAFS data from $[Os(\eta^2\text{-}H_2)(en)_2(O_2CCH_3)]PF_6$ (**XVI**) corresponded very well with those obtained from neutron diffraction (Os–H, 1.59, 1.60; H–H, 1.34 Å) and NMR spectroscopy (H–H, 1.27 Å). There were quite significant MS contributions to the XAFS from the Os–H–H pathways, despite the acute angles, which is no doubt due to the short Os–H and H–H distances. In addition, MS contributions involving the H atoms and atoms from the other ligands also contribute to the determination of the H–H distance [115].

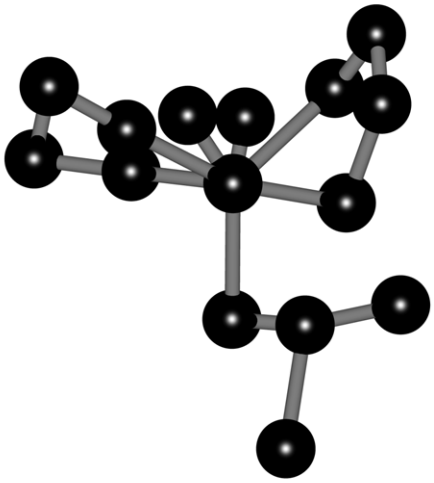

XVI

7. Dinitrogen complexes

As discussed in Section 2.1, MS contributions to XAFS are particularly strong in systems where atoms are nearly collinear, which makes it an ideal method for studying unstable dinitrogen complexes. The first example of this was the characterization of an unstable Mo dinitrogen intermediate, which was shown to have a linear dinuclear Mo–N≡N–Mo unit by MS analyses of XAFS data [119]. In particular, the near linear unit resulted in very strong contributions from the second N and Mo atoms from the absorbing atom, which made structure determination of such an intermediate from alternative structures very decisive [119]. Recently, the technique has been used to study unstable Ru and Os dinitrogen complexes (**XVII**) [115]. This is particularly powerful in the determination of the metal–ligand and N–N bond distances as a function of the metal ion and oxidation state in complexes that are disordered in crystals (i.e., mixed Ru–Os complexes), or very unstable (Os(III)–N_2 complexes). The oscillations caused by the linear Os–N≡N–Os or Os–N≡N–Ru moieties are so strong at the Os LIII edge that they only reach a maximum near the cut-off to the XAFS when it runs into the Os LII edge at ∼18 $Å^{-1}$ in the XAFS [115]. Such studies have provided valuable insights into the effects of different metal ions and oxidation states on π backbonding and what implications this might have for understanding nitrogen fixation [115].

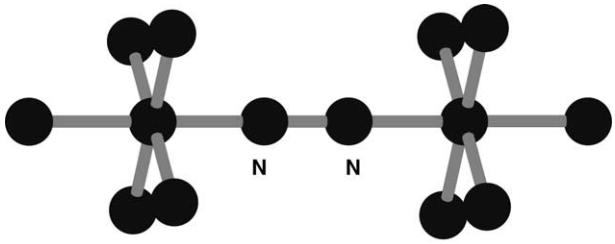

XVII

8. Conclusions

Multiple-scattering analysis of XAFS is a powerful technique for obtaining local three-dimensional structural information about an absorbing atom. It does not provide an absolute determination of structure for small molecules, or a three-dimensional structure of the whole protein in metalloproteins, in the same way that X-ray crystallography does. Nonetheless, MS analysis of XAFS data enables structural information to be obtained that is not possible to obtain via X-ray diffraction. In particular, XAFS can be obtained on any phase and even mixtures of compounds and is particularly useful at determining the three-dimensional structures of species that are too unstable to crystallize. This can be achieved by either rapid freezing of pure solutions of the complex of interest, or by rapid precipitation of the complex from mixtures followed by determination of the structure from microcrystalline or amorphous precipitates. In the case of metalloproteins, it should also be considered as a technique that provides complementary information to protein crystallography and NMR structure determinations. In particular, bond lengths and other geometric parameters about the absorbing atom are usually determined more precisely than is the case with protein crystallography [3,4]. MS analysis of XAFS data can also be used to determine the structure about the metal sites of metalloproteins that have not been characterized by NMR spectroscopy or protein crystallography, so long as sufficient information is known about the active site to build reasonable starting models.

While MS analysis of XAFS data is a powerful technique, it is also one that requires considerable care in obtaining high quality XAS data, the abstraction of data from the raw XAS, and analysis of the data thus obtained, in order to obtain a reliable structure determination. The procedures for doing this and problems that commonly arise are outlined in the previous sections.

Acknowledgments

We wish to acknowledge the many contributions of our coworkers and collaborators that are listed in the references. The research has been supported by the Australian Research Council (Large, Small, Discovery, SPIRT and LIEF grants), University of Sydney (Cancer Research Fund and Sesqui Grants), the Australian Synchrotron Research Program (ASRP) for access to the Australian National Beamline Facility (ANBF) in Tsukuba, Japan, and the Access to Major Facilities Program for access to the Stanford Synchrotron Radiation Laboratory (SSRL). The work was done (partially) at SSRL, which is operated by the Department of Energy, Office of Basic Energy Sources. The SSRL Biotechnology Program is supported by the National Institutes of Health, National Center for Research Resources, Biomedical Technology Program, and by the Department of Energy, Office of Biological and Environmental Research. The research at SSRL was funded by the Access to Major Facilities Program funded by the Department of Industry, Science and Resources and managed by the Australian Nuclear Science and Technology Organisation. Research was also performed at the ANBF with support from the ASRP, which is funded by the Commonwealth of Australia under the Major National Research Facilities program.

References

[1] E.I. Solomon, B. Hedman, K.O. Hodgson, A. Dey, R.K. Szilagyi, Coord. Chem. Rev. 249 (2005) 97.
[2] J.J. Rehr, A.L. Ankudinov, Coord. Chem. Rev. 249 (2005) 131.
[3] S.S. Hasnain, K.O. Hodgson, J. Synchrotron Radiat. 6 (1999) 852.
[4] S.S. Hasnain, R.W. Strange, J. Synchrotron Radiat. 10 (2003) 9.
[5] R.W. Strange, M. Ellis, S.S. Hasnain, Coord. Chem. Rev. 249 (2005) 197.
[6] A.M. Rich, R.S. Armstrong, P.J. Ellis, H.C. Freeman, P.A. Lay, Inorg. Chem. 37 (1998) 5743.
[7] A.M. Rich, R.S. Armstrong, P.J. Ellis, P.A. Lay, J. Am. Chem. Soc. 120 (1998) 10827.
[8] A.M. Rich, P.J. Ellis, L. Tennant, P.E. Wright, R.S. Armstrong, P.A. Lay, Biochemistry 38 (1999) 16491.
[9] M.-C. Cheng, A.M. Rich, R.S. Armstrong, P.J. Ellis, P.A. Lay, Inorg. Chem. 38 (1999) 5703.
[10] A. Weichsel, J.F. Andersen, D.E. Champagne, F.A. Walker, W.R. Montfort, Nat. Struct. Biol. 5 (1998) 304.
[11] E.A. Brucker, J.S. Olson, M. Ikeda-Saito, G.N. Phillips Jr., Proteins: Struct. Funct. Gen. 30 (1998) 352.
[12] D.M. Copeland, A.H. West, G.B. Richter-Addo, Proteins: Struct. Funct. Gen. 53 (2003) 182.
[13] X.A. Ding, A. Weichsel, J.F. Anderson, T.Kh. Shokhireva, C. Balfour, A.J. Pierek, B.A. Averill, W.R. Montfort, F.A. Walker, J. Am. Chem. Soc. 121 (1999) 128.
[14] A. Weichsel, J.F. Anderson, S.A. Roberts, W.R. Montfort, Nat. Struct. Biol. 7 (2000) 551.
[15] A. Di Cicco, J. Synchrotron Radiat. 10 (2003) 46.
[16] H.H. Zhang, B. Hedman, K.O. Hodgson, X-ray Absorption Spectroscopy and EXAFS Analysis: The Multiple-Scattering Method and Applications in Inorganic and Bioinorganic Chemistry, Inorganic Electronic Structure and Spectroscopy, vol. I, John Wiley & Sons Inc., New York, NY, 1999, p. 513.
[17] J.J. Rehr, A. Ankudinov, S.I. Zabinsky, Adv. Ser. Phys. Chem. 12B (2002) 1213.
[18] J. Penner-Hahn, in: J.A. McCleverty, T.J. Meyer (Eds.), Comprehensive Coordination Chemistry II, From Biology to Nanotechnology, vol. 2, Elsevier, Oxford, UK, 2004, Chapter 2.13, p. 159.
[19] P.J. Riggs-Gelasco, T.L. Stemmler, J.E. Penner-Hahn, Coord. Chem. Rev. 144 (1995) 245.
[20] S.P. Cramer, K.O. Hodgson, Prog. Inorg. Chem. 25 (1979) 1.
[21] S.J. Gurman, J. Synchrotron Rad. 2 (1995) 56.
[22] B.-K. Teo, in: A. Bianconi, L. Inoccia, S. Stipcich (Eds.), EXAFS and Near Edge Structure, Springer-Verlag, Berlin, 1983, p. 11.
[23] B.-K. Teo, J. Am. Chem. Soc. 103 (1981) 3990.
[24] N. Binsted, R.W. Strange, S.S. Hasnain, Biochemistry 31 (1992) 12117.
[25] S.S. Hasnain, R.W. Strange, in: S.S. Hasnain (Ed.), Synchrotron Radiation and Biophysics, Ellis Horwood Ltd., Chichester, 1990 (Chapter 4).
[26] T.E. Westre, A. Di Cicco, A. Filipponi, C.R. Natoli, B. Hedman, E.I. Solomon, K.O. Hodgson, Physica B 208–209 (1995) 137.
[27] T.E. Westre, A. Di Cicco, A. Filipponi, C.R. Natoli, B. Hedman, E.I. Solomon, K.O. Hodgson, J. Am. Chem. Soc. 117 (1995) 1566.
[28] M.J. Berger, J.H. Hubbell, S.M. Seltzer, J.S. Coursey, D.S. Zucker, XCOM, National Institute of Standards and Technology, Gaithersburg, MD, 1998, http://physics.nist.gov/PhysRefData/Xcom/Text/XCOM.html.
[29] A.M. Rich, Ph.D. Thesis, University of Sydney, 1997.
[30] S. Thomas, B.Sc. Hons Thesis, University of Sydney, 1999.
[31] C.A. Appleby, W.E. Blumberg, J. Peisach, B.A. Wittenberg, J.B. Wittenberg, J. Mol. Biol. 251 (1976) 6090.
[32] M. Sono, J.H. Dawson, Biochem. Biophys. Acta 789 (1984) 170.
[33] R.C. Farrow, J.H. Headspith, A.J. Dent, B.R. Dobson, R.L. Bilsborrow, C.A. Ramsdale, P.C. Stephenson, S. Brierley, G.E. Derbyshire, P. Sangsingkeow, K. Buxton, J. Synchrotron Rad. 5 (1998) 845.
[34] C. Karanfil, D. Chapman, G. Bunker, C. Segre, Rev. Sci. Instrum. 73 (2002) 1616.
[35] H. Oyanagi, C. Fonne, D. Gutknecht, P. Dressler, R. Henck, M.-O. Lampert, S. Ogawa, K. Kasai, S.B. Mohamed, Nucl. Instrum. Methods Phys. Res., Sect. A: Accel., Spectrom., Detect., Assoc. Equip. 513 (2003) 340.
[36] P.J. Ellis, H.C. Freeman, J. Synchrotron Rad. 2 (1995) 190.
[37] K.R. Bauchspie, Phys. B: Condensed Matter 208–209 (1995) 183.
[38] A. Levina, L. Zhang, P.A. Lay, Inorg. Chem. 42 (2003) 767.
[39] G.N. George, XAFSPAK, Stanford Synchrotron Research Laboratories, Stanford, CA, 2001, http://ssrl.slac.stanford.edu/exafspak.html.
[40] A. Kuzmin, EDA: EXAFS Data Analysis Software Package, Solid State Physics Institute, Riga, Latvia, 1999, http://www.dragon.lv/exafs.
[41] M. Tromp, M.Q. Slagt, R.J.M. Klein Gebbink, G. van Koten, D.E. Ramaker, D.C. Koningsberger, Phys. Chem. Chem. Phys. 6 (2004) 4397, and references therein.
[42] J.J. Rehr, C.H. Booth, F. Bridges, S.I. Zabinsky, Phys. Rev. B 49 (1994) 12347.
[43] H. Wende, P. Srivastava, R. Chauvistré, F. May, K. Baberschke, D. Arvanitis, J.J. Rehr, J. Phys.: Condensed Matter 9 (1997) L427.
[44] F. Bridges, C.H. Booth, G.G. Li, Phys. B: Condensed Matter 208–209 (1995) 137.
[45] J.J. Gurman, N. Binsted, I. Ross, J. Phys. C 19 (1986) 1845.
[46] A. Filipponi, A. Di Cicco, C.R. Natoli, Phys. Rev. B 52 (1995) 15122.
[47] A. Di Cicco, Physica B 209 (1995) 125.

[48] International XAFS Society, Survey of Error Analysis Procedures Used by Existing XAFS Software Packages, 1998, http://ixs.csrri.iit.edu/IXS/survey/errors/EA_Survey_Text.html.
[49] International XAFS Society, Error reporting recommendations: a report of the Standards and Criteria Committee, 2000, http://ixs.csrri.iit.edu/IXS/subcommittee_reports/sc/.
[50] A. Levina, P.A. Lay, Inorg. Chem. 43 (2004) 324.
[51] C.L. Weeks, A. Levina, C.T. Dillon, P. Turner, R.R. Fenton, P.A. Lay, Inorg. Chem., 43 (2004), in press.
[52] R. Ayala, E.S. Marcos, S. Díaz-Moreno, V.A. Solé, A. Muñoz-Páez, J. Phys. Chem. B 105 (2001) 7588.
[53] P.J. Merkling, A. Muñoz-Páez, E. Sanchez Marcos, J. Am. Chem. Soc. 124 (2002) 10911.
[54] J. Vojtechovský, K. Chu, J. Berendzen, R.M. Sweet, I. Schlichting, Biophys. J. 77 (1999) 2153.
[55] G.S. Kachalova, A.N. Popov, H.D. Bartunik, Science 284 (1999) 473.
[56] A.M. Rich, R.S. Armstrong, P.J. Ellis, P.A. Lay, L. Tennant, P.E. Wright, in preparation.
[57] L.J. Ignarro, C. Napoli, J. Loscalzo, Circ. Res. 90 (2002) 21.
[58] J. Torreilles, Frontiers Biosci. 6 (2001) D1161.
[59] M. Hoshino, L. Laverman, P.C. Ford, Coord. Chem. Rev. 187 (1999) 75.
[60] M.V. Beligni, L. Lamattina, Plant Cell Environ. 24 (2001) 267.
[61] M.-C. Cheng, Ph.D. Thesis, University of Sydney, 2000.
[62] J.B. Aitken, S.E. Thomas, R. Stocker, S.R. Thomas, O. Takikawa, R.S. Armstrong, P.A. Lay, Biochemistry 43 (2004) 4892.
[63] I.T. Bae, Y. Tolmachev, Y. Mo, D. Scherson, W.R. Scheidt, M.K. Ellison, M.-C. Cheng, R.S. Armstrong, P.A. Lay, Inorg. Chem. 40 (2001) 3256.
[64] I.C. Stefan, Y.B. Mo, S.Y. Ha, S. Kim, D. Scherson, Inorg. Chem. 42 (2003) 4316.
[65] G.R.A. Wyllie, W.R. Scheidt, Inorg. Chem. 42 (2003) 4259.
[66] M.K. Ellison, C.E. Schulz, W.R. Scheidt, J. Am. Chem. Soc. 124 (2002) 13833.
[67] J. Wang, W.S. Caughey, D.L. Rousseau, Resonance Raman scattering: a probe of heme protein-bound nitric oxide, in: M. Feelisch, J.S. Stamler (Eds.), Methods in Nitric Oxide Research, Wiley, 1996, Chapter 30, p. 427.
[68] R. Codd, C.T. Dillon, A. Levina, P.A. Lay, Coord. Chem. Rev. 216–217 (2001) 537.
[69] A. Levina, R. Codd, C.T. Dillon, P.A. Lay, Prog. Inorg. Chem. 51 (2003) 145.
[70] C.T. Dillon, P.A. Lay, B.J. Kennedy, A.P.J. Stampfl, Z. Cai, P. Ilinski, W. Rodrigues, D.G. Legnini, B. Lai, J. Maser, J. Biol. Inorg. Chem. 7 (2002) 640.
[71] C.T. Dillon, P.A. Lay, M. Cholewa, G.J.F. Legge, A.M. Bonin, T.J. Collins, K.L. Kostka, G. Shea-McCarthy, Chem. Res. Toxicol. 10 (1997) 533.
[72] M. Krumpolc, B. De Boer, J. Roček, J. Am. Chem. Soc. 100 (1978) 145.
[73] R.J. Judd, T.W. Hambley, P.A. Lay, J. Chem. Soc., Dalton Trans. (1989) 2205.
[74] A. Levina, G.J. Foran, P.A. Lay, J. Chem. Soc., Chem. Commun. (1999) 2339.
[75] A. Levina, R. Codd, G.J. Foran, T.W. Hambley, T. Maschmeyer, A.F. Masters, P.A. Lay, Inorg. Chem. 43 (2004) 1046.
[76] R. Codd, A. Levina, L. Zhang, T.W. Hambley, P.A. Lay, Inorg. Chem. 39 (2000) 990.
[77] M. Fainerman-Melnikova, Ph.D. Thesis, University of Sydney, 2002.
[78] C.M. Cawich, A. Ibrahim, K.L. Link, A. Bumgartner, M.D. Patro, S.N. Mahapatro, P.A. Lay, A. Levina, S.S. Eaton, G.R. Eaton, Inorg. Chem. 42 (2003) 6458.
[79] H.A. Headlam, C.L. Weeks, P. Turner, T.W. Hambley, P.A. Lay, Inorg. Chem. 40 (2001) 5097.
[80] P. Barnard, Ph.D. Thesis, University of Sydney, 2002.
[81] C.L. Weeks, Ph.D. Thesis, University of Sydney, 2001.
[82] S. Gez, R. Luxenhofer, A. Levina, R. Codd, P.A. Lay, Inorg. Chem., in preparation.
[83] D.I. Pattison, A. Levina, M.J. Davies, P.A. Lay, Inorg. Chem. 40 (2001) 214.
[84] E.S. Gould, Coord. Chem. Rev. 135 (1994) 651.
[85] R. Codd, P.A. Lay, A. Levina, Inorg. Chem. 36 (1997) 5440.
[86] A. Levina, unpublished results.
[87] P.A. Lay, A. Levina, Chromium, in: J.A. McLeverty, T.J. Meyer (Eds.), Comprehensive Inorganic Chemistry, vol. 3 (A.J. Wedd (Ed.)) Chapter 3.6, Elsevier, Oxford, UK, 2003, Chapter 4.6, p. 313.
[88] L. Jacquamet, Y. Sun, J. Hatfield, W. Gu, S.P. Cramer, M.W. Crowder, G.A. Lorigan, J.B. Vincent, J.-M. Latour, J. Am. Chem. Soc. 125 (2003) 774.
[89] A. Levina, P. Turner, P.A. Lay, Inorg. Chem. 42 (2003) 5392.
[90] L.R. Sharpe, W.R. Heineman, R.C. Elder, Chem. Rev. 90 (1990) 705.
[91] F. Villain, V. Briois, I. Castro, C. Helary, M. Verdaguer, Anal. Chem. 65 (1993) 2545.
[92] M.R. Antonio, L. Soderholm, I. Song, J. Appl. Electrochem. 27 (1997) 784.
[93] N.R.S. Farley, S.J. Gurman, A.R. Hillman, Electrochem. Commun. 1 (1999) 449.
[94] T. Yamaguchi, M. Valli, S. Miyata, H. Wakita, Anal. Sci. 13 (Suppl. S) (1997) 37.
[95] M.I. Bondin, G. Foran, S.P. Best, Aust. J. Chem. 54 (2001) 705.
[96] D.I. Pattison, P.A. Lay, M.J. Davies, Inorg. Chem. 39 (2000) 2729.
[97] D.I. Pattison, P.A. Lay, M.J. Davies, Redox Rep. 5 (2000) 130.
[98] D.I. Pattison, M.J. Davies, A. Levina, N.E. Dixon, P.A. Lay, Chem. Res. Toxicol. 14 (2001) 500.
[99] C.G. Pierpont, Proc. Ind. Acad. Sci., Chem. Sci. 114 (2002) 247.
[100] H.C. Chang, S. Kitagawa, Angew. Chem. Int. Ed. 41 (2002) 130.
[101] C.G. Pierpont, Inorg. Chem. 40 (2001) 5727.
[102] C.G. Pierpont, Coord. Chem. Rev. 219 (2001) 415.
[103] C.G. Pierpont, Coord. Chem. Rev. 216 (2001) 99.
[104] A. Levina, G.J. Foran, D.I. Pattison, P.A. Lay, Agnew. Chem. Int. Ed. Engl. 43 (2004) 462.
[105] J.H. Rodriguez, D.E. Wheeler, J.K. McCusker, J. Am. Chem. Soc. 120 (1998) 12051.
[106] J.E. Weder, C.T. Dillon, T.W. Hambley, B.J. Kennedy, P.A. Lay, J.R. Biffin, H.L. Regtop, N.M. Davies, Coord. Chem. Rev. 232 (2002) 95.
[107] C.T. Dillon, T.W. Hambley, B.J. Kennedy, P.A. Lay, J.E. Weder, Q. Zhou, Metal ions in biological systems, in: A. Sigel, H. Sigel (Eds.), Metal Ions and their Complexes in Medication, vol. 41, Marcel Dekker, Inc., New York, 2004 (Chapter 8).
[108] J.E. Weder, T.W. Hambley, B.J. Kennedy, P.A. Lay, D. MacLachlan, R. Bramley, C.D. Delfs, K.S. Murray, B. Moubaraki, B. Warwick, J.R. Biffin, H.L. Regtop, Inorg. Chem. 38 (1999) 1736.
[109] Y.R. Morgan, P. Turner, B.J. Kennedy, T.W. Hambley, P.A. Lay, J.R. Biffin, H.L. Regtop, B. Warwick, Inorg. Chim. Acta 324 (2001) 150.
[110] Q. Zhou, T.W. Hambley, B.J. Kennedy, P.A. Lay, P. Turner, B. Warwick, J.R. Biffin, H.L. Regtop, Inorg. Chem. 39 (2000) 3742.
[111] J.E. Weder, T.W. Hambley, B.J. Kennedy, P.A. Lay, G.J. Foran, A.M. Rich, Inorg. Chem. 40 (2001) 1295.
[112] J.E. Weder, Ph.D. Thesis, University of Sydney, 2000.
[113] Q. Zhou, T.W. Hambley, B.J. Kennedy, P.A. Lay, Inorg. Chem. 42 (2003) 8557.
[114] Q. Zhou, Ph.D. Thesis, University of Sydney, 2001.

[115] F. Chen, Ph.D. Thesis, University of Sydney, 2001.
[116] M.K. Oudenhuijzen, J.H. Bitter, D.C. Koningsberger, J. Phys. Chem. B 105 (2001) 4616.
[117] D.E. Ramaker, M. Teliska, Y. Zhang, A.Yu. Stakheev, D.C. Koningsberger, Phys. Chem. Chem. Phys. 5 (2003) 4492.
[118] T. Hasegawa, Z.W. Li, H. Taube, Chem. Lett. (1999) 7, and references therein.
[119] C.E. Laplaza, M.J.A. Johnson, J.C. Peters, A.L. Odom, E. Kim, C.C. Cummins, G.N. George, I.J. Pickering, J. Am. Chem. Soc. 118 (1996) 8623.